



A general calorimetry framework for measurement of combustion efficiency in a suppressed turbulent line fire



J.P. White^{*}, E.D. Link, A. Trouvé, P.B. Sunderland, A.W. Marshall

Department of Fire Protection Engineering, University of Maryland, College Park, MD 20742, USA

ARTICLE INFO

Keywords:

Calorimeter
Carbon dioxide generation
Extinction
Heat release rate
Oxygen consumption

ABSTRACT

The present study seeks to measure suppression effects in a canonical experimental configuration, featuring the exposure of a buoyant, turbulent, methane or propane-fueled diffusion flame to a co-flowing oxidizer diluted with nitrogen gas. Species-based calorimetry measurements, using either oxygen-consumption (OC) or carbon-dioxide-generation (CDG) based methods, are derived and applied to this configuration. Traditional OC models, which cannot account for oxidizer-dilution, are found to significantly overpredict total heat release rate in the present configuration, while traditional CDG models coincidentally give accurate results. Only the present calorimetry formulation, with full accommodation for oxidizer dilution, provides accurate results for both methods. In both methane and propane flames, global combustion efficiency is found to remain close to unity over a wide range of oxidizer dilution, decreasing abruptly only at the onset of global extinction. Similar trends are noted in the net combustion yields of oxygen, carbon-dioxide, and water-vapor. Net yields of carbon-monoxide remain close to zero for both fuels, but increase slightly near the extinction limit. These measurements reveal that despite visible suppression effects in all of the present flames, until the extinction limit is reached, nearly all of the fuel continues to react and combustion products are produced in stoichiometric proportions.

1. Introduction

In the field of fire safety, rate of heat release is often regarded as the most important parameter available to characterize a fire hazard [1]. This parameter can be useful and often essential in deriving various other fire properties including size, rate of growth/spread, material flammability, toxic species yields, suppression effectiveness, and combustion efficiency. Despite this importance, heat release rate can be difficult and costly to measure accurately, with a limited set of feasible measurement techniques available. Of the available techniques, species-based calorimetry is widely recognized as the most appropriate. By such methods, heat-release information is derived from the rates of consumption or production of the major chemical species involved in the combustion reaction.

The importance and empirical basis for species-based calorimetry has been well established in the literature. Notable review works have summarized the seminal and developmental studies leading to the establishment of these techniques [2,3]. Species-based calorimetry has been successfully applied in numerous studies ranging from small bench-scale applications [4–10], to large full-scale experiments [11–17]. These methods also form the basis of several national and international testing

standards for the determination of material flammability [18–21]. As in the present study, previous works have also explored the application of calorimetry measurements to characterize the combustion efficiency of suppressed fires [22–26]. Other studies have devoted to the characterization of the principal sources of uncertainty in the predominant calorimetry formulations [27–31].

While species-based calorimetry methods have been widely adopted by the fire testing and research communities and successfully employed in numerous studies, most of these implementations utilize simplified formulations that rely on specific and often unstated assumptions. In particular, most existing formulations apply only to simple systems where the primary mass exchanges to/from the combustion region are limited to the supply of fuel, entrainment of ambient air, and exhaust of combustion products. Certainly, this scenario adequately describes most fires, for which existing formulations have been shown to apply very well. However, for more complex systems with additional mass exchanges, such as those involving suppression agents or sprays, the existing formulations may not be applicable. The present study, which involves a co-flowing oxidizer with variable oxygen concentration, is a prime example of such a system.

Despite the wide body of existing literature, there is a limited

^{*} Corresponding author.

E-mail address: jwhite21@umd.edu (J.P. White).

availability of general guidelines to direct the design and implementation of calorimetry measurements in complex applications. As a result, it can be difficult to confidently extend the existing formulations to novel applications that may oppose their simplifying assumptions. One recent study has attempted to establish a modified calorimetry formulation and testing protocol applicable to a unique configuration with oxidizer dilution [32]. Though it provides some progress, the methodology advocated in that work lacks generality and requires unnecessary assumptions and limitations to the testing procedure. Clearly, additional guidance is needed to support the development of more generalized calorimetry formulations.

The present work seeks to fill this need by providing a comprehensive description of the physical principles underlying species-based calorimetry, developing from these principles a general framework for the design of calorimetry measurement systems, and demonstrating the successful implementation of such a system, within a configuration comprising complex mass exchanges that are incompatible with existing formulations.

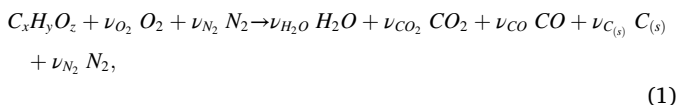
In the present configuration [33], a buoyant, turbulent diffusion flame is suppressed via diluted oxidizer stream. Species-based calorimetry techniques are developed and utilized within this configuration to assess flame-suppression response in both species yields and combustion efficiency across a range of conditions from complete combustion through total extinguishment. In addition to providing a basis for the development of the present calorimetry formulation, these measurements are useful in the pursuit of an improved understanding of suppression performance in realistic fire hazards.

2. Calculation

2.1. Combustion treatment

The foundation for species-based calorimetry is the thermodynamic concept that the heat released by a chemical reaction is directly related to the mass-rates of consumption and production of the major chemical species involved. In any species-based calorimetry application, it is necessary to first assume the combustion chemistry. The major species included in the assumed reaction determine which species must be considered in the enthalpy balance for the reaction, tracked in the mass conservation analysis that follows, and eventually measured in the calorimetry system.

Considering the combustion of a simple organic fuel in air, a global single-step reaction perspective gives



where ν_k are the molar reaction coefficients for each species, k , involved in the reaction. In this mechanism, an arbitrary fuel compound ($C_xH_yO_z$) and oxygen (O_2) are consumed to produce primarily water-vapor (H_2O) and carbon-dioxide (CO_2), while carbon-monoxide (CO) and soot ($C(s)$) are included as potential products of incomplete combustion. Nitrogen (N_2), along with any other inert species that may be present, is assumed to be globally unaffected by the reaction.

Detailed reaction kinetics are neglected in Eq. (1) via Hess's law, whereby the total enthalpy change over the course of a chemical reaction is independent of the reaction pathway. By the first law of thermodynamics, the enthalpy of reaction may then be equated to the heat of reaction, as long as the reaction occurs at constant pressure. The global perspective adopted in Eq. (1) is appropriate, so long as the primary species in the assumed mechanism indeed represent the major species present at the initial and final states of the reaction. Here, the initial state refers to an initially non-reacting fuel-oxidizer mixture and the final state

The mechanism in Eq. (1) should apply to most fire applications. For special applications in which there may be complex fuel chemistry, involvement of other reactive compounds, or any other factor leading to the net consumption or production of additional species in considerable quantities (H_2 , OH , NO_x , NH_3 , HCl , etc.), those species should be included in Eq. (1) and in the analysis that follows.

A significant advantage of species-based calorimetry is the well-reported observation that the heat released per-unit-mass of O_2 consumed in combustion reactions is approximately constant across wide variations in fuel chemistry [34–37]. As a result, species-based calorimetry may be applied with reasonable accuracy to characterize the combustion of unknown fuel compounds. Similar observations have been reported regarding the heat released per-unit-mass of CO_2 produced, leading to the establishment of two separate but similar methodologies. The former is referred to as oxygen-consumption (OC) calorimetry, and the latter as carbon-dioxide-generation (CDG) calorimetry.

While OC and CDG methods may have certain advantages and disadvantages in specific applications, their underlying formulations are similar. Based on the combustion chemistry assumed in Eq. (1), formulations for each method are given as

$$\dot{Q}_{OC} = -\Delta h_{O_2} \dot{\omega}_{O_2} + (\Delta h_{O_2} - \Delta h_{O_2, CO}) \left(\dot{\omega}_{CO} \frac{M_{O_2}}{2M_{CO}} \right) + (\Delta h_{O_2} - \Delta h_{O_2, C(s)}) \left(\dot{\omega}_{C(s)} \frac{M_{O_2}}{M_{C(s)}} \right), \quad (2a)$$

$$\dot{Q}_{CDG} = \Delta h_{CO_2} \dot{\omega}_{CO_2} + (\Delta h_{CO_2} - \Delta h_{CO_2, CO}) \left(\dot{\omega}_{CO} \frac{M_{CO_2}}{M_{CO}} \right) + (\Delta h_{CO_2} - \Delta h_{CO_2, C(s)}) \left(\dot{\omega}_{C(s)} \frac{M_{CO_2}}{M_{C(s)}} \right), \quad (2b)$$

where \dot{Q} is the combustion heat release rate, $\dot{\omega}_k$ is the mass reaction rate of species k , M_k is the molar mass of species k , and Δh_k is the mass-specific enthalpy of reaction for species k .

In particular, Δh_{O_2} and Δh_{CO_2} are the enthalpies of reaction for the assumed combustion mechanism (Eq. (1)) for complete combustion to CO_2 and H_2O (ν_{CO} , $\nu_{C(s)} = 0$), respectively per-unit-mass of O_2 consumed and CO_2 generated. Of the remaining terms, $\Delta h_{O_2, CO}$ ($\Delta h_{CO_2, CO}$) is the enthalpy of reaction for the oxidation of CO , given by the reaction $CO + 0.5 O_2 \rightarrow CO_2$, per-unit-mass of O_2 (CO_2), and $\Delta h_{O_2, C(s)}$ ($\Delta h_{CO_2, C(s)}$) is the enthalpy of reaction for the oxidation of soot, assumed to consist of pure graphitic carbon and given by the reaction $C(s) + O_2 \rightarrow CO_2$, per-unit-mass of O_2 (CO_2).

If the fuel chemistry is known, Δh_{O_2} and Δh_{CO_2} may be determined using Hess's law and a stoichiometrically balanced form of Eq. (1) (with ν_{CO} , $\nu_{C(s)} = 0$), with reference standard enthalpies of formation for the applicable product and reactant species ($\Delta \bar{h}_{f,k}$). This provides the most accurate (fuel-specific) determination of the enthalpy parameters, but requires prior knowledge of the fuel chemistry and its standard enthalpy of formation ($\Delta \bar{h}_{f,C_xH_yO_z}$). For applications where the required fuel properties are known, general expressions for determination of Δh_{O_2} and Δh_{CO_2} as a function of fuel properties are provided in Table 1.

For applications where fuel properties are unknown, Δh_{O_2} and Δh_{CO_2} may be approximated using average reference values, also provided in Table 1. These reference values represent the mean and standard deviation statistics for a collection of fuel-specific values determined by applying the general expressions in Table 1 to a list of roughly 150 hydrocarbon compounds comprising alkanes, alkenes, alkynes, arenes, alcohols, aldehydes, ketones, and esters (see Tables 3–4.12 and 3–4.13 in Ref. [37] for the list of compounds). These reference values should only be used when fuel properties are unknown, but still expected to be well represented by this group of compounds. As shown, the standard

Table 1
Expressions and reference values (MJ/kg) for enthalpy parameters in Eq. (2), including fuel-specific values for CH₄ and C₃H₈.

Parameter	Expression (per Eq. (1))	Reference	CH ₄	C ₃ H ₈
Δh_{O_2}	$\frac{z}{2} \frac{\Delta \bar{h}_{H_2O} + x \Delta \bar{h}_{CO_2} - \Delta \bar{h}_{C_3H_8}}{(x + \frac{z}{2}) M_{O_2}}$	12.9±0.24	12.54	12.77
Δh_{CO_2}	$\frac{z}{2} \frac{\Delta \bar{h}_{H_2O} + x \Delta \bar{h}_{CO_2} - \Delta \bar{h}_{C_3H_8}}{x M_{CO_2}}$	13.4±1.1	18.23	15.48
$\Delta h_{O_2, CO}$	$\frac{2(\Delta \bar{h}_{CO_2} - \Delta \bar{h}_{CO})}{M_{O_2}}$	17.69	–	–
$\Delta h_{O_2, C(s)}$	$\frac{\Delta \bar{h}_{CO_2} - \Delta \bar{h}_{C(s)}}{M_{O_2}}$	12.30	–	–
$\Delta h_{CO_2, CO}$	$\frac{\Delta \bar{h}_{CO_2} - \Delta \bar{h}_{CO}}{M_{CO_2}}$	6.43	–	–
$\Delta h_{CO_2, C(s)}$	$\frac{\Delta \bar{h}_{CO_2} - \Delta \bar{h}_{C(s)}}{M_{CO_2}}$	8.94	–	–

deviation in the reference value for Δh_{O_2} is notably less than that for Δh_{CO_2} , so that the OC formulation may typically be expected to give more accurate results for applications with unknown fuel composition (provided $\dot{\omega}_O$ and $\dot{\omega}_{CO_2}$ are both measured with similar accuracy).

Experiments in the present study are conducted using pure methane (CH₄) and propane (C₃H₈) fuels. Since the properties for these fuels are known, fuel-specific values for Δh_{O_2} and Δh_{CO_2} are used, as provided in Table 1. Note that Table 1 also includes general expressions and reference values for $\Delta h_{O_2, CO}$, $\Delta h_{O_2, C(s)}$, $\Delta h_{CO_2, CO}$, and $\Delta h_{CO_2, C(s)}$. These four parameters are unaffected by fuel chemistry and may therefore be treated as configuration-independent constants.

The expressions in Eq. (2) primarily comprise the product of a mass reaction rate and an enthalpy of reaction for the appropriate reacting species (O₂ for OC and CO₂ for CDG), with additional terms included to account for incomplete combustion to CO and C_(s). Here, production of CO or C_(s) (instead of CO₂) yields a net decrease in the combustion heat release, due to the resulting reductions in O₂ consumption and CO₂ generation, as well as the smaller (less negative) enthalpies of formation for CO and C_(s) products compared to CO₂.

It is important to note that the expressions in Eq. (2) uniquely apply to the combustion chemistry assumed in Eq. (1), and that for applications where other species are consumed or produced in considerable quantities, Eqs. (1) and (2) must both be reformulated to reflect the applicable reaction chemistry.

2.2. Mass conservation analysis

Once the combustion mechanism and applicable enthalpy parameters are determined, the primary duty of a calorimetry measurement system is then the accurate evaluation of the species reaction rates ($\dot{\omega}_k$) in Eq. (2), which may be derived via mass conservation analysis. A model control volume is depicted in Fig. 1 for a simple open combustion system comprising a fuel source (\dot{m}^f) placed beneath an exhaust collection system (\dot{m}^e) with ambient air entrainment (\dot{m}^a). For the configuration of interest in the present study, an additional mass source is included representing a co-flowing oxidizer around the fuel source (\dot{m}^{ox}). Systems lacking this source may simply ignore associated terms in the expressions that follow. More complex systems may also be considered, where additional or alternative mass exchanges must then be added to the control volume and the expressions that follow. It is essential that the assumed control volume completely characterize all unique compositions of mass exchanged across its boundaries.

Conservation of total mass within the control volume gives

$$0 = \sum_j \dot{m}^j + \frac{dm}{dt}, \quad (3)$$

where \dot{m}^j is the mass flow rate of stream *j* across the boundary of the control volume, *m* is the total mass contained in the control volume, and *t* is time. The dm/dt term in Eq. (3) accounts for the accumulation or

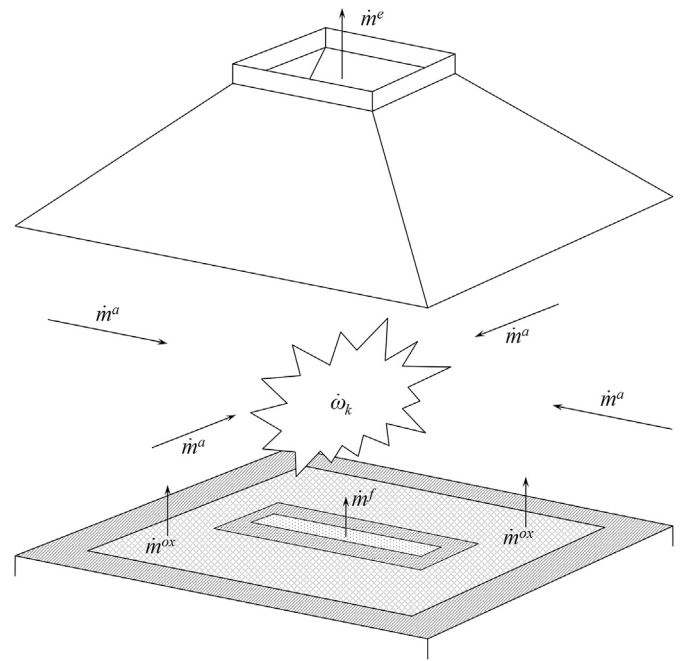


Fig. 1. Control volume for a simple open combustion system comprising a fuel source (\dot{m}^f) beneath an exhaust collection system (\dot{m}^e) with ambient air entrainment (\dot{m}^a), co-flowing oxidizer (\dot{m}^{ox}), and chemical reaction source ($\dot{\omega}_k$). All of \dot{m}^f , \dot{m}^a , \dot{m}^{ox} , and $\dot{\omega}_k$ are assumed totally captured within \dot{m}^e .

reduction of mass within the control volume due to unsteady flow at the boundaries. This term is typically important only for very large systems where the flow-through time of the control volume is significantly greater than the measurement timescales of interest. Recent studies have explored calorimetry measurements in applications where such dm/dt effects are important, with limited success [11,16,17].

For the present configuration and including a steady-state assumption where dm/dt effects are neglected, Eq. (3) simplifies to

$$\dot{m}^e = \dot{m}^f + \dot{m}^a + \dot{m}^{ox}, \quad (4)$$

where it is additionally assumed that there be no loss of mass from the system except through the exhaust flow. As most system designs include measurement instrumentation in the exhaust stream, this limitation ensures that all products of combustion are collected and measured. Alternative configurations are possible, but may considerably complicate measurement requirements.

Conservation of species mass in the control volume gives

$$\dot{\omega}_k = \sum_j \dot{m}_k^j + \frac{dm_k}{dt}, \quad (5)$$

where $\dot{\omega}_k$ is the mass reaction rate of species *k*, \dot{m}_k^j is the mass flow rate of species *k* within flow stream *j*, and m_k is the mass of species *k* contained in the control volume. As before, a steady-state assumption applied to the present configuration simplifies Eq. (5) to

$$\dot{\omega}_k = \dot{m}_k^e - \dot{m}_k^a - \dot{m}_k^{ox}. \quad (6)$$

It is typically appropriate to further simplify Eq. (6) through assumptions that limit the constituent species in each stream. For example, the fuel stream usually consists of pure fuel and products of incomplete combustion are usually negligible in the ambient. Still, some applications may feature complex or diluted fuel mixtures or significant ambient vitiation. In general, all species that may be present in each stream should be considered.

Species mass flow rates within each stream may be expressed in terms

of the stream composition via

$$\dot{m}_k^j = X_k^j \dot{m}^j \frac{M_k}{M^j}, \quad (7)$$

where X_k^j is the mole fraction of species k within stream j , M_k is the molar mass of species k , and M^j is the mixed molar mass of stream j , which can also be expressed in terms of the stream composition as

$$M^j = \sum_k (X_k^j M_k), \quad (8)$$

provided that

$$\sum_k X_k^j = 1, \quad (9)$$

must also be satisfied.

By application of Eq. (4), the mass flow rate of one stream may be directly obtained provided the others are known. Typically, \dot{m}^a is difficult or impossible to measure, and all \dot{m}^j except \dot{m}^a should therefore be measured. Alternatively, assuming non-reactivity of N_2 ($\dot{\omega}_{N_2} = 0$), Eq. (6) may be re-written as

$$\dot{m}_{N_2}^a = \dot{m}_{N_2}^e - \dot{m}_{N_2}^f - \dot{m}_{N_2}^{ox}, \quad (10)$$

and inserted into an inverted form of Eq. (7), written as

$$\dot{m}^a = \frac{\dot{m}_{N_2}^a}{X_{N_2}^a} \frac{M^a}{M_{N_2}}. \quad (11)$$

When available, Eqs. (10) and (11) typically provide a more accurate determination of \dot{m}^a , than direct use of Eq. (4), with the stipulation that $\dot{m}_{N_2}^j$ must be measured or estimated for all N_2 -containing flow streams (which usually also requires measurement of all \dot{m}^j except \dot{m}^a). This measurement requirement may be burdensome for complex configurations, but the advantage provided by this complexity is that \dot{m}^a is determined dynamically, responding to any measured changes in both the composition and flow rate of each stream. Formulations similar to Eqs. (10) and (11) may also be derived for applications where other inert species may be present.

A similar simplification is noted in Eq. (9), where X_k^j for one of the constituent species in each flow stream, considered as the background species, may be obtained provided the others are known. In the exhaust and ambient, N_2 is typically the most appropriate species to omit measurement, and thus all species except N_2 should be measured for these streams. Selected background species for any additional flow streams may vary depending on their composition.

An additional mass conservation statement may also be applied to the combustion reaction, giving

$$\sum_k \dot{\omega}_k = 0, \quad (12)$$

which states that there can be no net change in mass within the control volume due to chemical reaction. This equation may be used as a simple check on mass conservation to verify that all $\dot{\omega}_k$ indeed sum to zero, but is perhaps more useful as a means of obtaining $\dot{\omega}_k$ for one species provided all others are known. Though useful, this calculation is more difficult to implement than the preceding simplifications, requiring an iterative procedure where the composition of the unmeasured species must first be estimated in order to determine $\dot{\omega}_k$ for the others. For this reason, Eq. (12) is not used in the present analysis.

2.3. Measurement considerations

Eqs. (3)–(12) provide the necessary framework for any calorimetry

measurement system, where the desired species reaction rates, $\dot{\omega}_k$, as appear in Eq. (2), may be determined from measurements of the compositions (X_k^j) and total mass flow rates (\dot{m}^j) of the applicable mass exchanges in the system. Additional considerations for the measurement of these quantities are discussed as follows.

In a typical calorimetry system, composition instrumentation is installed in the exhaust stream using an extractive sampling system leading to various species analyzers. For most analyzers, the flow sample must be conditioned via filtration to remove soot and other particulates and a combination of cold-traps and desiccation to remove H_2O . Note that Drierite™, which is the most appropriate desiccant for H_2O removal in calorimetry applications, is known to also interact with CO_2 and can impede CO_2 measurement response in samples with transient CO_2 content [38,39]. The amount of Drierite™ used for sample conditioning should be minimized to alleviate such effects.

The removal of any species from the sample presents additional challenge because the analyzer-measured sample composition sans the removed species does not accurately represent the true stream composition. Analyzer composition measurements must then be corrected to account for sample conditioning via

$$X_k^j = X_{k,A}^j \left(1 - \sum_{k, rmv} X_k^j \right), \quad (13)$$

where $X_{k,A}^j$ is the analyzer-measured mole fraction of species k in the stream j sample. The summation in Eq. (13) is performed over any species k that is removed from the sample during conditioning (usually only H_2O removal is necessary), where X_k^j for any such species must be directly measured via either in situ sensors or extractive analyzers installed upstream of the applicable sample conditioning.

Mass flow rates may be measured by numerous techniques, the proper choice of which depends on the applicable flow characteristics. For high-flow, low-pressure conditions, as typically encountered in calorimetry exhaust systems, differential-pressure methods are preferred, where a differential-pressure sensing device is placed in the applicable flow stream and the flow rate is determined as

$$\dot{m}^j = C_f^j A^j \left(\frac{2 \Delta P^j P^j M^j}{R T^j} \right)^{1/2}, \quad (14)$$

where A^j is the cross-sectional area of the flow stream, ΔP^j is the sensor-measured differential pressure, P^j is the static pressure of the flow, T^j is the temperature of the flow, M^j is the molar mass of the flow mixture, R is the ideal gas constant, and C_f^j is a flow coefficient characterizing the velocity profile across the cross-section of the stream. All of these quantities are evaluated at the location of the probe.

Note that Eq. (14) relies on Bernoulli's principle to relate the measured differential pressure to the flow velocity, hence compressibility effects are neglected. The flow velocity is related to the mass flow rate via the flow density, which is estimated from the stream composition, pressure, and temperature via the ideal gas law. As a result, condensed-phase contributions to the exhaust mass, such as soot and other particulates or condensed forms of H_2O are neglected.

The flow coefficient, C_f^j , may be determined by calibrating the differential-pressure sensor to a condition with known flow rate. A suitable procedure may include adding an accurately measured flow of some species into the applicable flow stream, while accurately measuring the downstream concentration of that species (after mixing) using an available species analyzer. The total flow rate may then be obtained by relating the known species flow rate to the background flow rate required to yield the measured concentration. Differential-pressure sensors with a known and constant flow coefficient are also available and require no calibration.

A number of previous works have advocated the treatment of C_f^j as a

calibration factor applicable to the entire calorimetry model, whereby C_f^j is determined by placing a calibration burner with known heat release rate into the measurement system. The value of C_f^j is then fixed so that the model returns the correct heat release rate. This type of calibration procedure should be avoided because it combines any and all extraneous factors affecting the measurement into a single factor that has no physical relationship to many of the effects that may be included (such as unintentional loss of combustion products). Such effects may vary for measuring conditions different from the calibration test, potentially resulting in significant unidentifiable errors in the measurements. For these reasons, it is highly recommended that C_f^j be determined via independent flow calibration (as described in the preceding paragraph) and not using a calibration burner.

2.4. Model sensitivity

An analysis examining the relative sensitivity of the present calorimetry formulation to its principal input quantities is summarized in Table 2. Model sensitivity is evaluated in terms of a sensitivity factor, S , defined as

$$S_{\dot{Q}} = \frac{\Delta\dot{Q} / \dot{Q}}{\Delta\phi / \phi}, \tag{15}$$

where $\Delta\phi$ is an arbitrary change in any input quantity ϕ , and $\Delta\dot{Q}$ is the resulting change in the model output \dot{Q} . For $S_{\dot{Q}} = 1$, a 10% relative variation in ϕ yields a 10% relative variation in \dot{Q} . Note that the S values provided in Table 2 are unique to the specific measured conditions cited in Table 2 and may vary significantly for other conditions. As shown, maximum S for the OC formulation are significantly greater than those for the CDG formulation for the cited measured condition. This is primarily due to the fact that $X_{O_2}^a \gg X_{CO_2}^a$ relative to the change in X_k^e for each species that occurs due to combustion. For the measured condition cited in Table 2, $\dot{Q}_{OC} \approx \dot{Q}_{CDG} \approx 50$ kW.

While the S values in Table 2 cannot be generalized quantitatively, they may be qualitatively interpreted to indicate the relative sensitivity of the formulation to certain input quantities compared to others. As expected, the OC formulation is most sensitive to the applicable O_2 mole fractions in the control volume ($X_{O_2}^j$), the exhaust flow rate (\dot{m}^e), and Δh_{O_2} . Similarly, the CDG formulation is most sensitive to the exhaust CO_2 mole fraction ($X_{CO_2}^e$), \dot{m}^e , and Δh_{CO_2} . These quantities should be prioritized for accurate measurement in applications where highly accurate determinations of \dot{Q} are desired.

Table 2
Sensitivity analysis of the present calorimetry formulation; sensitivity factors, $S_{\dot{Q}}$, define the ratio of change in the output \dot{Q} to an arbitrary change in each input quantity.

Parameter	Value	$S_{\dot{Q}_{oc}}$	$S_{\dot{Q}_{cdg}}$
\dot{m}^e	0.850 kg/s	1.04	1.00
$X_{O_2}^e$	0.197 mol/mol	- 60.7	0.05
$X_{CO_2}^e$	0.002 mol/mol	- 0.16	1.23
$X_{H_2O}^e$	0.037 mol/mol	- 0.03	- 0.03
X_{CO}^e	0.000 mol/mol	< 0.01	< 0.01
\dot{m}^{ox}	0.085 kg/s	- 0.04	< 0.01
$X_{O_2}^{ox}$	0.205 mol/mol	6.05	- 0.03
$X_{O_2}^a$	0.205 mol/mol	55.9	- 0.06
$X_{CO_2}^a$	0.000 mol/mol	0.03	- 0.23
$X_{H_2O}^a$	0.016 mol/mol	< 0.01	< 0.01
Δh_{O_2}	12.54 MJ/kg	1.00	-
Δh_{CO_2}	18.23 MJ/kg	-	1.00
$\Delta h_{O_2, CO}$	17.69 MJ/kg	< 0.01	< 0.01
$\Delta h_{CO_2, CO}$	6.43 MJ/kg	< 0.01	< 0.01

2.5. Summary

The principal tenants of the present calorimetry framework are described in the following.

- (1) Assume some form of the global combustion chemistry, as in Eq. (1).
- (2) Determine the enthalpy parameters to be used in Eq. (2), using either balanced stoichiometric calculations or average reference values.
- (3) Develop a control volume based mass conservation analysis that considers all of the relevant mass exchanges in the applicable configuration and from that analysis, derive configuration-specific forms of Eqs. (3) and (5), analogous to those in Eqs. (4) and (6).
- (4) With considerations for Eqs. (7)–(14), determine the appropriate instrumentation necessary to close the system of Eqs. (3)–(14), including any necessary modifications for specific applications.

The solution procedure for the present calorimetry model is depicted as a block diagram in Fig. 2. The procedure requires first the determination of the compositions of all applicable flow streams using an appropriate configuration of species analyzers. This includes measuring X_k^j for any species removed during sample conditioning, measuring $X_{k,A}^j$ for all remaining species, correcting all $X_{k,A}^j$ via Eq. (13), obtaining X_k^j for the selected background species in each stream via Eq. (9), and determining each M^j via Eq. (8). Next, \dot{m}^j for all applicable flow streams (typically with the exception of \dot{m}^a) are either directly measured or are determined via Eq. (14). Using the now available M^j , \dot{m}^j , and X_k^j , available \dot{m}_k^j are obtained via Eq. (7). Typically unavailable for direct measurement, \dot{m}^a is obtained via Eqs. (10) and (11) using all $\dot{m}_{N_2}^j$. Next, all \dot{m}_k^a

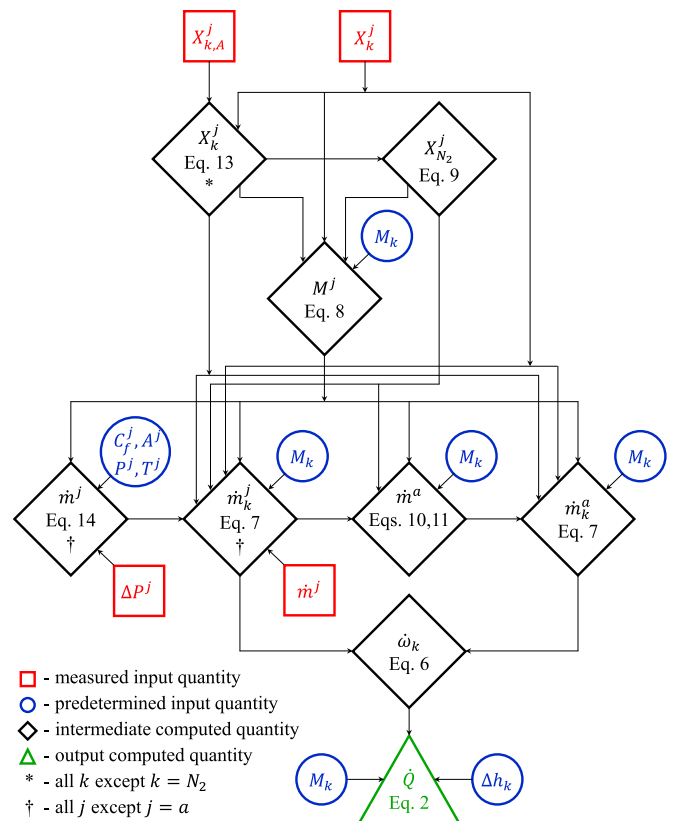


Fig. 2. Block diagram depicting the solution procedure for the present calorimetry framework.

are determined via Eq. (7). With all \dot{m}_k^i now available, the desired $\dot{\omega}_k$ are determined via Eq. (6). Finally, \dot{Q} is obtained via Eq. (2) using the appropriately determined Δh_k .

General assumptions necessary for any species-based calorimetry application follow.

- (1) The assumed global reaction chemistry comprises all major species present in *considerable* quantities before and after the reaction.
- (2) The reaction occurs at constant pressure.
- (3) The control volume completely characterizes all unique compositions of mass exchanged across its boundaries.
- (4) The reaction occurs entirely within the control volume.

Optional simplifying assumptions applied to the present model also include the following. Omission of these assumptions may be possible, but could considerably complicate the analysis. Further simplifications are available, but would require additional assumptions.

- (5) The global reaction chemistry follows that given in Eq. (1).
- (6) Nitrogen is conserved and unaffected by the reaction.
- (7) Soot consists of pure graphitic carbon.
- (8) All flow streams crossing the boundaries of the control volume are quasi-steady, and therefore mass accumulation and reduction within the control volume is neglected.
- (9) No mass is lost from the system (except that exiting through the monitored exhaust stream).
- (10) All flow compositions are well-mixed at the locations in which they are measured.
- (11) The derivation of Eq. (14) neglects compressibility effects and assumes ideal gas behavior, also neglecting the mass contributions of any condensed-phase species to the mixed stream density.

The calorimetry framework presented in the preceding sections has been derived to be as generally applicable as possible within the limitations of the previously listed assumptions. As necessary, some features of the formulation are specifically applicable to the configuration of interest in this study, consisting of a suppressed open flame configuration with a co-flowing oxidizer stream diluted with inert gas. Fig. 1 and Eqs. (4), (6) and (10) reflect this specific configuration. The preceding framework may be readily extended to other configurations by substituting Fig. 1 for a control volume applicable to the configuration of interest and from that control volume developing appropriate forms of Eqs. (4), (6) and (10). The remaining expressions and solution procedures may then be followed as described in Fig. 2.

The present calorimetry framework provides notable advancements over traditional formulations presented in previous works [22,31,40–46]. In particular, most traditional formulations have sought to coalesce and simplify their solutions as much as possible to yield what comes close to a single algebraic expression for heat release rate as a function of directly measured quantities. These simplifications are achieved through convoluted algebraic manipulations requiring the definition of additional model parameters in an oxygen-depletion factor, defined as the fraction of incoming air that is fully depleted of its oxygen, and an expansion coefficient, defined as the ratio of the number of moles in the fraction of air fully depleted of its oxygen to the number of moles of combustion products. These quantities are undesirable due to their ambiguous physical significance, limited applicability to specific configurations, and because they have no legitimate relationship to the calculation of the heat release rate, as evidenced by their feasible omission from the present framework. In particular, the expansion coefficient is relevant only when conservation statements are written as a mole basis instead of a mass basis and may be accurately defined only for cases where the fuel chemistry is known.

While simplified formulations may be more convenient for hand

calculations, they suffer the ambiguity of being far-removed from the mass conservation analysis that led to their derivation. As a result, these formulations are not easily adaptable to conditions that deviate from those for which they were originally derived. Further, the conditions for which these formulations were originally derived are also not easily inferred from their final formulations.

Using similar simplification methods, it would be possible to derive from the present model an explicit expression for \dot{Q} as a function of directly measured quantities; however, this would not be prudent as such an expression would be unintelligibly complex while offering questionable benefit. Rather, the simple expressions presented in Eqs. (3)–(14) need only be performed in the proper sequence as shown in Fig. 2, providing an easily programmable solution procedure adaptable to any data analysis or spreadsheet program. Most importantly, these simple expressions are directly relatable to their underlying physical principles and to the configuration for which they were derived, offering transparency to the model formulation and the underlying assumptions. The present formulation is also readily adaptable to alternative configurations that may require mass conservation analyses of greater or lesser complexity.

3. Experiment

The present experimental facility is described in Ref. [33] and illustrated in Fig. 3. This facility features a 5-cm-wide by 50-cm-long fuel port

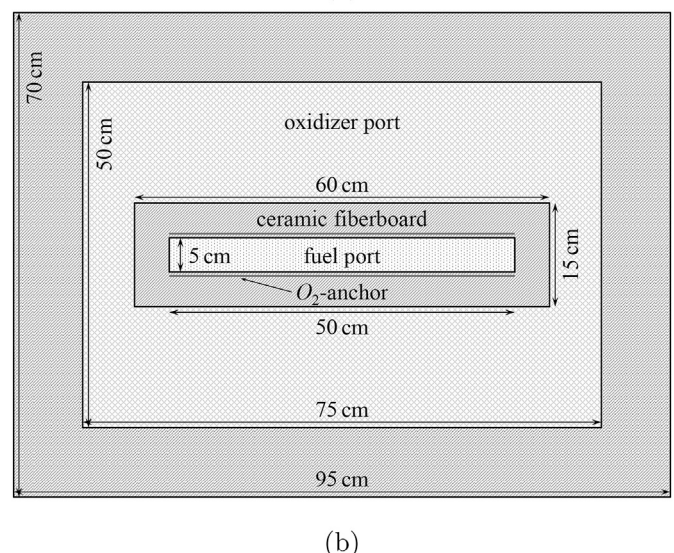
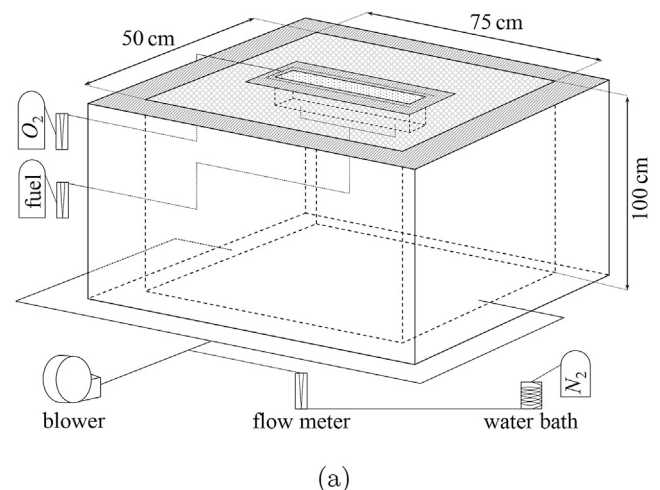


Fig. 3. (a) Diagram of experimental facility. (b) Plan-view of fuel/oxidizer port surface.

centrally located within a 50-cm-wide by 75-cm-long co-flowing oxidizer port. Surrounding the fuel port is a thin 5-cm-wide strip of ceramic fiberboard, which promotes transition to fully turbulent flow conditions at the flame base (see Fig. 3b). A methane flow of 1.00 ± 0.02 g/s or a propane flow of 1.08 ± 0.02 g/s, measured via mass flow controller, yields flames with unsuppressed total heat release of roughly 50 kW. The co-flowing oxidizer flows at a fixed rate of 85 ± 7 g/s, including a variable flow of gaseous nitrogen to provide controlled flame suppression via reduction in the O_2 mole fraction of the oxidizer ($X_{O_2}^{ox}$).

As noted in previous works, weakened flames in co-flow may lift and detach from the fuel port prior to extinction [33,47–49]. To prevent liftoff extinction events and permit the study of substantially weakened flames, an O_2 anchor is optionally applied along the fuel port to strengthen the flame base (see Fig. 3b). A constant flow of O_2 at 0.080 ± 0.0008 g/s provides less than 2.0% of the stoichiometric O_2 requirement for either fuel and has been shown to sufficiently prevent liftoff extinction [33]. Present experiments including this O_2 flow are referred to as ‘anchored’, while those without are referred to as ‘non-anchored’, with all other testing conditions being the same between the two cases.

The experimental apparatus (Fig. 3a) is centrally positioned roughly 1.1 m beneath a 2 m by 2 m fire-products collection hood connected to an exhaust evacuation system. A 60-cm-tall fiberglass curtain hangs from the perimeter of the hood to ensure total capture of all combustion products into the exhaust system. Preliminary experiments lacking this curtain were found to suffer significant loss of combustion products, leading to underestimation of calorimetry-derived heat release rates in excess of 20%. The necessity for inclusion of this curtain in the present configuration stresses the importance of assumption (9) in the preceding calorimetry model.

Within the exhaust system, measurement sensors are contained within a 3-m-long straight section of 0.28 m inner-diameter round duct. All sensors are located roughly 5.2 m (18.5 diameters) downstream of the collection hood, such that sufficiently fully-developed and well-mixed flow conditions may be assumed.

A Veris Verabar V100 averaging pitot-tube ($C_f^j = 0.7530$) connected to a Setra Model 264 differential-pressure transducer is used to measure the exhaust flow rate with an uncertainty of $\pm 1\%$. Adjacent to the pitot-tube, an exposed-junction K-type thermocouple probe measures the exhaust temperature with an uncertainty of ± 2 K and response time of roughly 3 s.

A Michell Instruments PCMini52 relative humidity sensor is used to measure the exhaust H_2O content in situ with an uncertainty of $\pm 1\%$ RH and response time of roughly 10 s. The measured relative humidity is related to absolute humidity via a thermodynamic state equation for the saturation pressure of H_2O as a function of temperature [50].

A sampling probe collects a portion of the exhaust flow for extractive composition measurements. The sampling probe consists of a 4.5 mm inner-diameter stainless-steel tube with 1.5 mm perforations spaced 1.27 cm uniformly along its length, running the full diameter of the exhaust duct. A vacuum pump draws the exhaust sample from both ends of the probe, through a length of 3.2 mm inner-diameter tubing toward the species analysis instrumentation. The sample passes through a 2- μ m particulate filter, a section of Drierite™ desiccant, and an additional 2- μ m filter prior to analysis.

Extractive composition measurements include O_2 content via a Rosemount Model 755 paramagnetic analyzer and CO_2 and CO content via a Siemens ULTRAMAT 23 non-dispersive infrared analyzer. Measurement uncertainties are ± 1250 ppm O_2 , ± 1000 ppm CO_2 , and ± 100 ppm CO , with a response time of roughly 5 s for both analyzers. No soot data are measured in the present study, and associated terms in Eq. (2) are therefore neglected. The exhaust sampling system is additionally used to measure the ambient composition, assumed to remain constant at initial condition measured prior to each experiment.

In the oxidizer, $X_{O_2}^{ox}$ is measured using a Servomex 540E paramagnetic

analyzer via a sampling probe located in the oxidizer port, with measurement uncertainty of ± 1250 ppm O_2 and response time of roughly 5 s. The remaining oxidizer composition is determined by assuming a uniform mixture of ambient air with pure N_2 . Measurements of $X_{O_2}^{ox}$ are then directly related to the mole fractions of H_2O , CO_2 , and CO in the oxidizer based on the measured composition of those species in the ambient.

The oxidizer flow rate is measured using a United Sensor pitot-static probe ($C_f^j = 0.8972$) with uncertainty of $\pm 8\%$, calibrated by flowing known amounts of N_2 through the oxidizer while measuring resultant changes in $X_{O_2}^{ox}$. As in the exhaust stream, an exposed-junction K-type thermocouple probe measures the oxidizer temperature with an uncertainty of ± 2 K and response time of roughly 3 s. For anchored experiments, the O_2 flow introduced by the anchor is directly included as an additional term in Eqs. (4) and (6) of the calorimetry model.

Prior to each experiment, all species analyzers are calibrated against reference mixtures with known composition to ensure measurement accuracy and minimize effects of calibration drift. Measurement response delays, due to differences in flow transport time to the various instruments, are also compensated to provide synchronous data collection across all measurements. Uncertainties in all calorimetry-derived quantities are estimated using a Monte-Carlo error propagation analysis [51].

4. Results and discussion

4.1. Model performance

The principal difference between the present calorimetry formulation and those provided in previous works is a consideration for complex mass exchanges such as the present configuration’s diluted oxidizer. To explore this distinction, total heat release rates (\dot{Q}), derived using input data measured in the present configuration and using both present and traditional models, are plotted versus the O_2 mole fraction of the oxidizer, $X_{O_2}^{ox}$, in Fig. 4 for OC and Fig. 5 for CDG based methods. Model variants include (1) the present formulation; (2) the present formulation, but with the oxidizer mass flow rate, $\dot{m}^{ox} = 0$ within the model so as to artificially remove the influence of the diluted oxidizer; and (3) a traditional formulation for either OC [41] or CDG [43] based methods.

As shown in Fig. 4, \dot{Q} for all three OC models converge only at ambient $X_{O_2}^{ox}$, with models (2) and (3) remaining in close agreement for all $X_{O_2}^{ox}$. This agreement verifies that the present formulation converges with the traditional formulation when the diluted oxidizer is neglected. Notably, models (2) and (3) significantly overpredict \dot{Q} , with deviations between these models and the reference model (1) increasing linearly

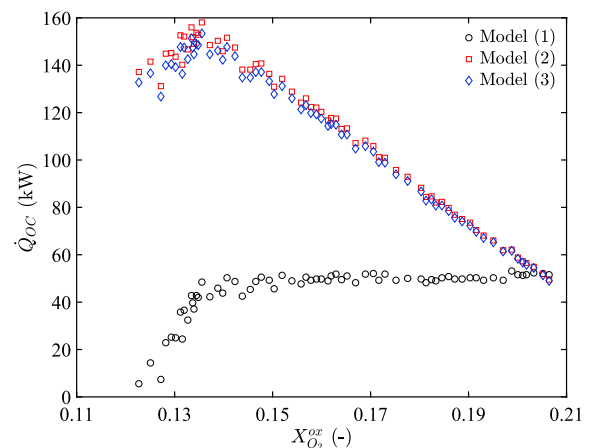


Fig. 4. Comparison of \dot{Q}_{OC} versus $X_{O_2}^{ox}$ among varying calorimetry formulations for an anchored methane flame. Selected models include (1) the present formulation with measured \dot{m}^{ox} , (2) the present formulation with $\dot{m}^{ox} = 0$, and (3) a traditional OC formulation [41].

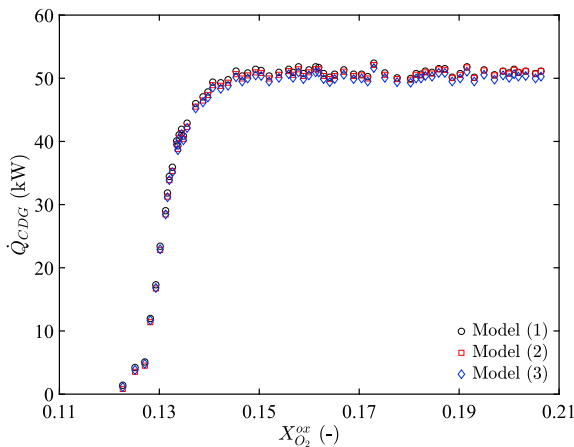


Fig. 5. Comparison of \dot{Q}_{CDG} versus $X_{O_2}^{ox}$ among varying calorimetry formulations for an anchored methane flame. Selected models include (1) the present formulation with measured \dot{m}^{ox} , (2) the present formulation with $\dot{m}^{ox} = 0$, and (3) a traditional CDG formulation [43].

with declining $X_{O_2}^{ox}$. This trend is due to the sensitivity of the OC formulation to the O_2 content of the oxidizer, which directly impacts the O_2 mass balance central to OC calorimetry. In particular, as $X_{O_2}^{ox}$ is reduced, the O_2 deficit in the exhaust due to dilution of the oxidizer begins to dominate that due to O_2 consumption in the flame. As models (2) and (3) cannot account for oxidizer dilution, they incorrectly attribute the entire exhaust O_2 deficit to the combustion reaction, resulting in vastly over-predicted \dot{Q} .

The linear deviation of models (2) and (3) away from model (1) is explained by the roughly linear dependence of $\dot{m}_{O_2}^{ox}$ on $X_{O_2}^{ox}$. Since the total oxidizer mass flow rate (\dot{m}^{ox}) remains constant, $\dot{m}_{O_2}^{ox}$ decreases linearly with the declining O_2 mass fraction of the oxidizer ($Y_{O_2}^{ox}$), and therefore also decreases quasi-linearly with declining $X_{O_2}^{ox}$ (non-linearity in the relationship between $Y_{O_2}^{ox}$ and $X_{O_2}^{ox}$ is negligible over the range of $X_{O_2}^{ox}$ shown in Fig. 4).

Contrary to the noted discrepancies in the OC formulations, \dot{Q} for all three CDG models converge for all $X_{O_2}^{ox}$ (see Fig. 5). This agreement is due to the relative insensitivity of the CDG formulation to dilution in the oxidizer, where the CO_2 content of the oxidizer is nearly negligible and does not deviate significantly from that in the ambient. As a result, variations in $X_{O_2}^{ox}$ do not significantly impact the CO_2 mass balance of the system, and surplus CO_2 in the exhaust is consistently dominated by that generated in the flame. Hence, models (2) and (3) maintain accurate predictions for \dot{Q} , despite neglecting the diluted oxidizer.

While the preceding comparisons may suggest superiority of the CDG over the OC formulation, it must be noted that such a conclusion is configuration dependent. If, for example, oxidizer dilution in the present configuration were accomplished via CO_2 instead of N_2 addition, the CDG formulation would expectedly be significantly more sensitive to dilution of the oxidizer. For such a scenario, the traditional CDG formulation would not be expected to yield accurate results.

The model comparisons in Fig. 4 emphasize the importance of a comprehensive control volume analysis in the derivation of any calorimetry formulation, where the undue omission of applicable mass exchanges may significantly affect the accuracy of the model. However, comparisons in Fig. 5 highlight that for complex systems, not all applicable mass exchanges need significantly influence both the OC and CDG formulations. Careful consideration of the species mass balances in a given calorimetry application may provide a useful means to determine a priori which formulation should be preferred and whether any omission of measurements may be acceptable.

4.2. Suppression measurements

OC and CDG calorimetry-derived \dot{Q} (see Eq. (2)) are plotted versus $X_{O_2}^{ox}$ in Fig. 6. Individual plots present data for the non-anchored methane (Fig. 6a), anchored methane (Fig. 6b), non-anchored propane (Fig. 6c), and anchored propane (Fig. 6d) flames. Also included in each plot are the corresponding combustion efficiency data, defined as

$$\eta_{comb} = \frac{\dot{Q}}{\dot{m}_f \Delta h_f}, \quad (16)$$

where \dot{m}_f is the measured input mass flow of fuel and Δh_f is the enthalpy of combustion per-unit-mass of fuel.

As shown in Fig. 6, $\dot{Q}_{OC} \approx \dot{Q}_{CDG}$ for all $X_{O_2}^{ox}$ and for all four flames, indicating good agreement between the two methods, as should be expected with the present model. Also shown, uncertainties in \dot{Q}_{OC} and \dot{Q}_{CDG} are initially comparable (± 1.5 kW) near ambient $X_{O_2}^{ox}$, but deviate with declining $X_{O_2}^{ox}$. Uncertainty in \dot{Q}_{OC} gradually increases, eventually and significantly exceeding that in \dot{Q}_{CDG} (± 11 kW max for \dot{Q}_{OC} vs. ± 2 kW max for \dot{Q}_{CDG}). This trend is principally due to the heightened sensitivity of \dot{Q}_{OC} to uncertainties in the oxidizer composition and flow rate (see Table 2).

Also shown in Fig. 6, $\eta_{comb} \approx 1$ for all four flames over a wide range of reduced $X_{O_2}^{ox}$. For the non-anchored flames (Fig. 6a and c), η_{comb} tapers only slightly, lowering to a value of roughly 0.8 for both fuels immediately before global extinction. For these flames, extinction occurs as detachment of the flame from the fuel port and subsequent liftoff. The value of $X_{O_2}^{ox}$ at extinction is denoted the limiting oxygen index (LOI , shown as a vertical dotted line in each figure), with presently measured LOI for the non-anchored flames (LOI_{na}) of 0.152 ± 0.002 for methane and 0.139 ± 0.002 for propane, values in agreement with prior measurements [33].

For the anchored flames (Fig. 6b and d), and for $X_{O_2}^{ox} > LOI_{na}$, \dot{Q} and η_{comb} are equivalent to those measured for the respective non-anchored flames for each fuel. For $X_{O_2}^{ox} < LOI_{na}$, the O_2 anchor extends the domain of flammability, where \dot{Q} and η_{comb} reduce gradually with declining $X_{O_2}^{ox}$ until global extinction. For the anchored flames, extinction occurs as increasingly intermittent quenching of the main flame until only a small pilot flame remains in the immediate vicinity of the anchor, extinguishing shortly thereafter. Presently measured LOI for the anchored flames (LOI_a) are 0.122 ± 0.002 for methane and 0.125 ± 0.002 for propane. A further discussion of these extinction limits and comparison with similar limits measured in other configurations has been provided in previous work [33].

From the measured species mass reaction rates ($\dot{\omega}_k$, see Eq. (6)), net combustion yields are defined as

$$y_k = \frac{\dot{\omega}_k}{\dot{m}_f}. \quad (17)$$

Measured y_k for O_2 , CO_2 , H_2O , and CO are plotted versus $X_{O_2}^{ox}$ in Fig. 7. As before, individual plots present data for the non-anchored methane (Fig. 7a), anchored methane (Fig. 7b), non-anchored propane (Fig. 7c), and anchored propane (Fig. 7d) flames. Included in each plot are the stoichiometric yields for each species (shown as horizontal dashed lines), defined as

$$y_{k,st} = \nu_{k,st} \frac{M_k}{M_f}, \quad (18)$$

where M_k is the molar mass of species k , M_f is the molar mass of the fuel, and $\nu_{k,st}$ is the stoichiometric molar reaction coefficient for species k in the balanced combustion mechanism (see Eq. (1)).

As shown in Fig. 7, $y_k \approx y_{k,st}$ for all species and for all four flames over a wide range of reduced $X_{O_2}^{ox}$. As expected, trends in y_{O_2} and y_{CO_2} closely

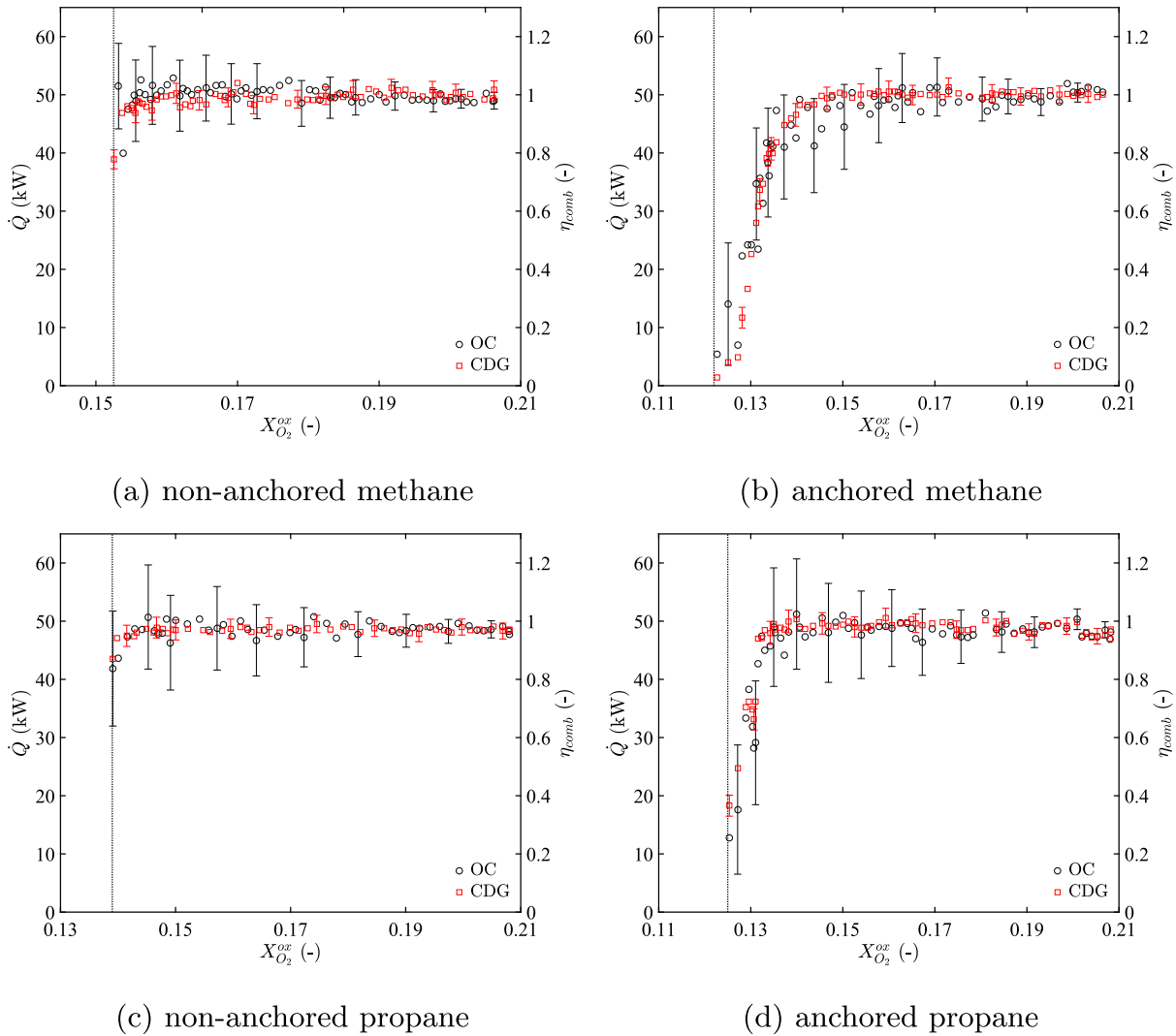


Fig. 6. OC and CDG calorimetry-derived heat release rate (\dot{Q}) and combustion efficiency (η_{comb}) plotted versus $X_{O_2}^{ox}$ for various flames.

match those noted for the \dot{Q}_{OC} and \dot{Q}_{CDG} measurements (see Fig. 6). Trends in y_{H_2O} resemble those for y_{O_2} and y_{CO_2} , though with significantly greater measurement uncertainty. Uncertainty in y_{H_2O} is principally attributed to the relative inaccuracy of the H_2O sensor, as compared to the highly accurate analyzers used for the other species. Despite the relatively high uncertainty, measured y_{H_2O} reasonably match $y_{H_2O,st}$ for the present flames. As has been reported in previous works [22,28,31,44], the OC and CDG calorimetry formulations are relatively insensitive to uncertainty in the H_2O measurements, therefore the noted uncertainty in y_{H_2O} does not significantly affect the other calorimetry-derived quantities.

For all four flames, measured $y_{CO} \approx 0$. For the non-anchored flames (Fig. 7a and c), a small but nearly negligible increase in y_{CO} is noted at the moment of global extinction. A more notable and prolonged increase in y_{CO} is measured for the anchored flames (Fig. 7b and d), where $y_{CO} > 0$ only for $X_{O_2}^{ox} < LOI_{na}$, increasing with declining $X_{O_2}^{ox}$ until reaching maxima of $y_{CO,max} = 0.045$ at $X_{O_2}^{ox} = 0.132$ for methane and $y_{CO,max} = 0.022$ at $X_{O_2}^{ox} = 0.128$ for propane. With further reduction in $X_{O_2}^{ox}$, y_{CO} for either fuel diminishes as extinction effects begin to dominate any incomplete combustion.

Related to the sensitivity of the calorimetry formulation, the contribution of CO production to the total \dot{Q} remains minor even at the peak y_{CO} shown in Fig. 7b. For the OC formulation in Eq. (2a), the contribution

of \dot{w}_{CO} to the total \dot{Q}_{OC} is less than 0.26%, whereas for the CDG formulation in Eq. (2b), the contribution of \dot{w}_{CO} to the total \dot{Q}_{CDG} is less than 2.63%. Here, the CDG formulation is more sensitive to \dot{w}_{CO} than the OC formulation because the difference $\Delta h_{CO_2} - \Delta h_{CO_2, CO}$ in Eq. (2b) is typically much larger in magnitude than the difference $\Delta h_{O_2} - \Delta h_{O_2, CO}$ in Eq. (2a) (see values in Table 1). Though other potential combustion species such as H , H_2 , and OH are not considered in this study, these species are expected to have considerably lower yields than CO [52], with negligible effect on the determination of \dot{Q} .

Based on experimental observations of the anchored flames, it is suspected that the regime of increasing y_{CO} and decreasing y_{CO_2} measured just before global extinction indicates the presence of spatially separated regions in the flame zone where some portion of the injected fuel reacts to completion, forming primarily CO_2 and H_2O , while other portions of the injected fuel fail to ignite and pass unreacted into the exhaust. The increasing y_{CO} trend suggests that there are some intermediate regions between these two extremes where incomplete combustion occurs, though the relatively small magnitude of y_{CO} compared to y_{CO_2} indicates that these effects are not significant and that complete combustion and extinction occur in a somewhat binary fashion in the present flames. As a result, any observed reduction in global η_{comb} in the present configuration more likely indicates spatially localized flame extinction rather than globally inefficient combustion. This behavior is consistent with expectations from laminar flamelet extinction and percolation

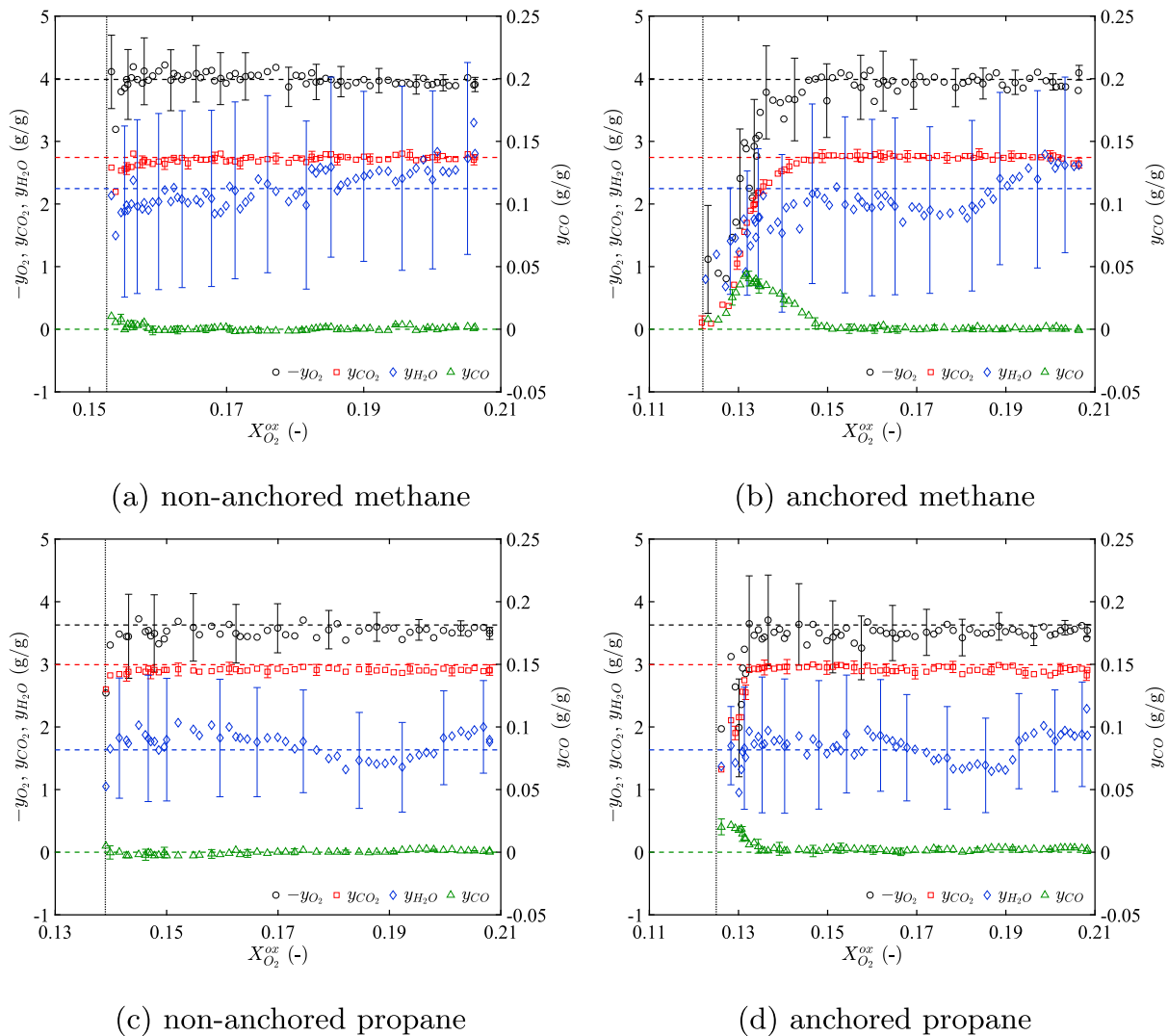


Fig. 7. Net combustion yields (y_k) for O_2 , CO_2 , H_2O , and CO plotted versus $X_{O_2}^{ox}$ for various flames.

theories [53,54], though it should be noted that detailed investigations of these phenomena in buoyant, turbulent fires have not yet been performed.

Previous experimental work in the present configuration has demonstrated that the flames of interest in this study do experience significant variations in visible flame structure and radiative emissions with declining $X_{O_2}^{ox}$ [33]. Notably, both methane and propane flames exhibit a significant reduction in luminous emissions combined with a transition in flame color from yellow to blue as $X_{O_2}^{ox}$ is reduced (see Figs. 5 and 6 in Ref. [33]). Simultaneously, those flames exhibit a roughly linear decline in radiative loss fraction (χ_{rad}) with decreasing $X_{O_2}^{ox}$ (see Figs. 9 and 10 in Ref. [33]).

Despite these other suppression effects, the present data conclude that for all of the present flames and for $X_{O_2}^{ox} > LOI_{na}$, nearly all of the fuel continues to react to completion and combustion products are produced in stoichiometric proportions. These results agree with speculations reported in previous studies [55–57], for which locally measured species concentrations suggested the persistence of complete combustion until the extinction limit, but validating combustion efficiency measurements were not provided. The present results establish a definitive confirmation of these behaviors.

To further investigate the significance of these results, the presently measured η_{comb} are compared against the previously measured χ_{rad} data, which are included in Fig. 8, reproduced from Figs. 9 and 10 in Ref. [33]

(the reader is referred to Ref. [33] for a description of the χ_{rad} measurement). Considering the measured trends in these two quantities (η_{comb} remain constant near unity and χ_{rad} decline linearly with reducing $X_{O_2}^{ox}$), it is apparent that when combined, both trends should occur with a concomitant increase in the convective fraction of the total heat release, χ_{conv} .

A measured estimate of χ_{conv} is plotted in Fig. 8, defined as

$$\chi_{conv} = \frac{\dot{m}^e c_p^e (T^e - T^a)}{\dot{m}_f \Delta h_f}, \quad (19)$$

where \dot{m}^e is the mass flow rate, T^e the temperature, and c_p^e the heat capacity of the combustion exhaust gases, with other terms as previously defined. Here, c_p^e is estimated as the corresponding value for ambient air, evaluated at temperature T^e . Also included in Fig. 8 is the sum,

$$\chi_{sum} = \chi_{conv} + \chi_{rad}. \quad (20)$$

As shown in Fig. 8, measured χ_{conv} increase quasi-linearly with declining $X_{O_2}^{ox}$ for all four flames, due primarily to associated increases in T^e . The increasing trend in χ_{conv} is nearly perfectly offset by the decreasing trend in χ_{rad} , so that χ_{sum} closely matches η_{comb} . The χ_{sum} trend slightly, but consistently under-predicts the η_{comb} trend, attributed to heat losses that are not accounted for in the χ_{conv} and χ_{rad} measurements. Such

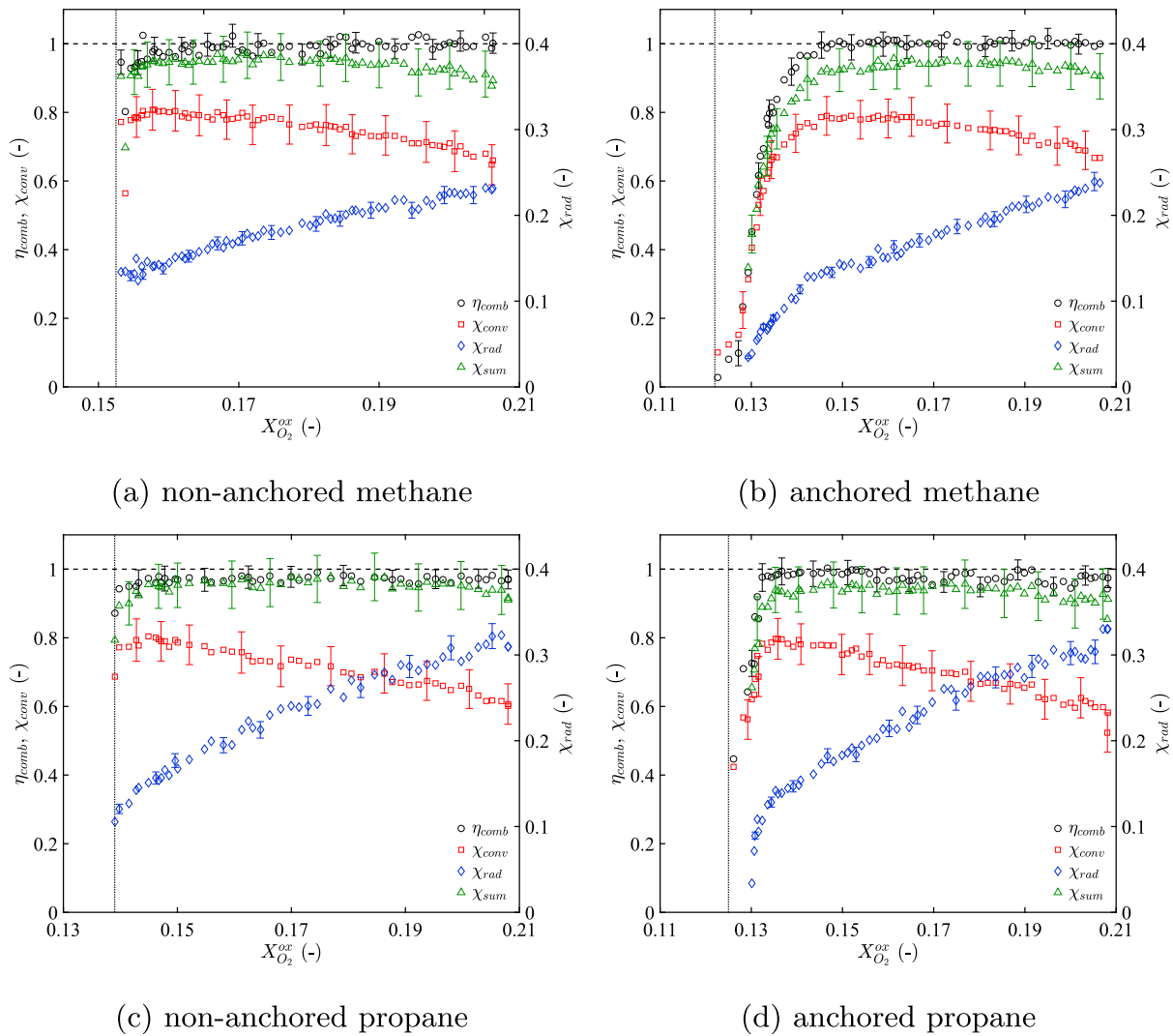


Fig. 8. Comparison of η_{comb} (calorimetry derived), χ_{rad} (thermally derived), and χ_{conv} (thermally derived) plotted versus $X_{O_2}^{ox}$ for various flames.

losses likely include conduction losses at the flame base to the burner or additional losses to the walls of the exhaust system. In comparing the offset between η_{comb} and χ_{sum} , these losses are suggested to be small and unaffected by declining $X_{O_2}^{ox}$, though such agreement is likely configuration dependent.

The agreement between the present η_{comb} and χ_{sum} measurements offers two additional conclusions. First, χ_{sum} , which is based entirely on thermal measurements, provides an independent validation of the species-based calorimetry principles used to evaluate η_{comb} , where the calorimetry-derived heat release rate is determined using mass-conservation analyses and species measurements only and includes no actual thermal measurements.

Second, because of the complexity required for species-based calorimetry measurements, the present results suggest that coupled measurements of χ_{rad} and χ_{conv} may provide an attractive and inexpensive alternative method for global heat release rate measurements, particularly for cases where qualitative trends are desired and a systematic offset in quantitative result due to heat losses may be acceptable. For suppression studies in particular, qualitative η_{comb} trends inferred from χ_{conv} and χ_{rad} measurements may potentially be calibrated to yield quantitative results, provided η_{comb} at an unsuppressed condition is known and any offset due to heat losses may be assumed to be independent of suppression effects.

Summarizing the present experimental results, it is expected that the

primary effect of the diluted oxidizer is to reduce the flame temperature, where the increasing presence of inert N_2 in the reacting mixture dissipates the heat released by combustion. Because radiative flame emissions scale with temperature to the fourth power, χ_{rad} is most sensitive to this effect and reduces quasi-linearly with declining $X_{O_2}^{ox}$. Despite the reducing flame temperature, η_{comb} has been found to remain close to unity until the extinction limit is reached, suggesting a constant rate of heat release into the reacting mixture. With less of that heat lost to radiation, a greater fraction is convected away from the flame into the plume, resulting in increased plume and exhaust temperatures. This behavior is consistent with laminar extinction theory and the existence of a cutoff temperature above which combustion is primarily stable and proceeds to completion, but below which combustion cannot occur.

5. Conclusion

A general formulation for species-based calorimetry measurements using either oxygen-consumption (OC) or carbon-dioxide-generation (CDG) based methods has been presented. While not as convenient as the simplified models offered in previous works, the present formulation is directly relatable to the physical principles from which it is derived, offering transparency to its derivation and underlying assumptions. This formulation may also be more easily adapted to complex applications opposing the simplifying assumptions in traditional models. The present

study features the application of this formulation to a canonical configuration featuring buoyant, turbulent, methane or propane-fueled diffusion flames, suppressed via diluted co-flowing oxidizer.

Traditional OC-based models, which cannot account for oxidizer dilution, are found to significantly overpredict total heat release rate in the present configuration. By comparison, traditional CDG-based models are found to give accurate results, but only because the CO_2 mass balance in the present configuration is not significantly influenced by N_2 dilution of the oxidizer. For an alternate scenario in which the oxidizer is diluted with excess CO_2 instead of N_2 , agreement would not be expected. Only the present formulation, with full accommodation for oxidizer dilution, provides accurate prediction of total heat release rate via both OC and CDG methods.

As emphasized by the present model comparisons, the undue omission of applicable mass exchanges in the derivation of any calorimetry formulation may significantly affect model accuracy. Careful consideration of the species mass balances in a given application may provide a useful means to determine a priori whether OC or CDG formulations

should be preferred.

In both methane and propane flames, combustion efficiency is found to remain close to unity over a wide range of oxidizer dilution, decreasing rapidly only at the onset of global extinction. Similar trends are noted in the net combustion yields of O_2 , CO_2 , and H_2O . Net yields of CO remain close to zero for both fuels, but increase slightly near the extinction limit. Despite other suppression effects noted in these flames, until the extinction limit is reached, nearly all fuel continues to react and combustion products are produced in stoichiometric proportions.

Acknowledgments

This project is supported by the U.S. National Science Foundation (NSF-GOALI Award #1236788), with additional support from collaborators at FM Global and United Technology Research Center. Discussions with S. Vilfayeau, T. Myers, H.-Z. Yu, and Y. Wang are gratefully acknowledged. Special thanks are given to T. Western for assistance in the design and construction of the calorimetry facilities.

Nomenclature

Symbols

A	area (m^2)
c_p	heat capacity ($J/kg/K$)
C_f	flow coefficient (–)
LOI	limiting oxygen index (mol/mol)
m	mass (kg)
\dot{m}	mass flow rate (kg/s)
M	molar mass (kg/mol)
P	static pressure (Pa)
\dot{Q}	heat release rate (W)
R	ideal gas constant ($J/mol/K$)
S	sensitivity factor (–)
t	time (s)
T	temperature (K)
X	mole fraction (mol/mol)
y	net combustion yield (kg/kg)
Δh	mass-specific enthalpy of reaction (J/kg)
$\Delta \bar{h}_f$	mole-specific standard enthalpy of formation (J/mol)
ΔP	differential pressure (Pa)
η_{comb}	combustion efficiency (–)
ν	molar reaction coefficient (mol/mol)
ϕ	model input quantity (–)
χ_{rad}	radiative loss fraction (–)
χ_{conv}	convective loss fraction (–)
χ_{sum}	total loss fraction (–)
$\dot{\omega}$	mass reaction rate (kg/s)

Subscripts

a	anchored
A	analyzer measured
CDG	carbon dioxide generation
f	fuel species
k	indexing variable (species)
max	maximum
na	non-anchored
OC	oxygen consumption
rmv	removed
st	stoichiometric

Superscripts

a	ambient entrainment
-----	---------------------

e	exhaust stream
f	fuel stream
j	indexing variable (flow stream)
ox	oxidizer stream

References

- [1] V. Babrauskas, R.D. Peacock, Heat release rate: the single most important variable in fire hazard, *Fire Saf. J.* 18 (3) (1992) 255–272.
- [2] K.D. Steckler, Estimation of rate of heat release by means of oxygen consumption measurements, in: D.R. Lide (Ed.), *A Century of Excellence in Measurements, Standards, and Technology*, CRC Press, 2001, pp. 280–282.
- [3] J.R. Lawson, SFPE classic paper review: a review of classic work by Dr William J. Parker on heat release rate measurements by oxygen consumption, *J. Fire Prot. Eng.* 22 (2012) 5–9.
- [4] V. Babrauskas, Development of the cone calorimeter—a bench-scale heat release rate apparatus based on oxygen consumption, *Fire Mater.* 8 (2) (1984) 81–95.
- [5] H.C. Tran, R.H. White, Burning rate of solid wood measured in a heat release rate calorimeter, *Fire Mater.* 16 (4) (1992) 197–206.
- [6] S. Brohez, G. Marlair, C. Delvosalle, Fire calorimetry relying on the use of the fire propagation apparatus. Part I: early learning from use in Europe, *Fire Mater.* 30 (2) (2006) 131–149.
- [7] S. Brohez, G. Marlair, C. Delvosalle, Fire calorimetry relying on the use of the fire propagation apparatus. Part II: burning characteristics of selected chemical substances under fuel rich conditions, *Fire Mater.* 30 (1) (2006) 35–50.
- [8] H. Biteau, A. Fuentes, G. Marlair, S. Brohez, J.L. Torero, Ability of the fire propagation apparatus to characterise the heat release rate of energetic materials, *J. Hazard. Mater.* 166 (2) (2009) 916–924.
- [9] P. Ribière, S. Grugeon, M. Morcrette, S. Boyanov, S. Laruelle, G. Marlair, Investigation on the fire-induced hazards of Li-ion battery cells by fire calorimetry, *Energy Environ. Sci.* 5 (2012) 5271–5280.
- [10] C. Fourneau, C. Delvosalle, H. Breulet, S. Brohez, Characterization of highly under-ventilated fires using the cone calorimeter, *Fire Mater.* 40 (3) (2016) 434–444.
- [11] J.S. Newman, C. Wieczorek, J.M. Troup, Application of building-scale calorimetry, in: *Fire Safety Science—Proceedings of the Eighth International Symposium, IAFSS, 2005*, pp. 1425–1434.
- [12] S.C. Kim, M. Bundy, Numerical model of a large-scale oxygen consumption fire calorimeter, *J. Therm. Anal. Calorim.* 93 (3) (2008) 1013–1019.
- [13] A. Hamins, E. Johnsson, M. Donnelly, A. Maranghides, Energy balance in a large compartment fire, *Fire Saf. J.* 43 (3) (2008) 180–188.
- [14] P.-A. Santoni, F. Morandini, T. Barboni, Determination of fireline intensity by oxygen consumption calorimetry, *J. Therm. Anal. Calorim.* 104 (3) (2011) 1005–1015.
- [15] Y.J. Ko, R. Michels, G.V. Hadjisophocleous, Instrumentation design for HRR measurements in a large-scale fire facility, *Fire Technol.* 47 (4) (2011) 1047–1061.
- [16] H. Pretrel, W. Le Saux, L. Audouin, Determination of the heat release rate of large scale hydrocarbon pool fires in ventilated compartments, *Fire Saf. J.* 62 (2013) 192–205.
- [17] H. Pretrel, W. Le Saux, L. Audouin, Experimental determination of fire heat release rate with OC and CDG calorimetry for ventilated compartments fire scenario, *Fire Mater.* 38 (4) (2014) 474–506.
- [18] ASTM E1354–16a, Standard Test Method for Heat and Visible Smoke Release Rates for Materials and Products Using an Oxygen Consumption Calorimeter, ASTM International, 2016. www.astm.org.
- [19] ASTM E2058–13a, Standard Test Methods for Measurement of Material Flammability Using a Fire Propagation Apparatus (FPA), ASTM International, 2013. www.astm.org.
- [20] ASTM E2067–15, Standard Practice for Full-scale Oxygen Consumption Calorimetry Fire Tests, ASTM International, 2015. www.astm.org.
- [21] ISO 5660-1:2015, Reaction-to-fire Tests – Heat Release, Smoke Production and Mass Loss Rate – Part 1: Heat Release Rate (Cone Calorimeter Method) and Smoke Production Rate (Dynamic Measurement), ISO, 2015. www.iso.org.
- [22] B.Z. Dlugogorski, J.R. Mawhinney, V. Huu Duc, The measurement of heat release rates by oxygen consumption calorimetry in fires under suppression, in: *Fire Safety Science—Proceedings of the Fourth International Symposium, IAFSS, 1994*, pp. 877–888.
- [23] J. Qin, B. Yao, W.K. Chow, Experimental study of suppressing cooking oil fire with water mist using a cone calorimeter, *Hosp. Manag.* 23 (5) (2004) 545–556.
- [24] J. Qin, W.K. Chow, Bench-scale tests on PMMA fires with water mist, *Polym. Test.* 24 (1) (2005) 39–63.
- [25] W.K. Chow, J. Qin, S.S. Han, Bench-scale tests on controlling plastic fires with water mists, *Chem. Eng. Technol.* 28 (9) (2005) 1041–1047.
- [26] J. Qin, W.K. Chow, S.S. Han, Bench-scale studies on suppressing ghee fires with water mist, in: *Fire Safety Science—Proceedings of the Tenth International Symposium, IAFSS, 2011*, pp. 111–118.
- [27] R.W. Yeager, Uncertainty analysis of energy release rate measurement for room fires, *J. Fire Sci.* 4 (4) (1986) 276–296.
- [28] P.A. Enright, C.M. Fleischmann, Uncertainty of heat release rate calculation of the ISO 5660-1 cone calorimeter standard test method, *Fire Technol.* 35 (2) (1999) 153–169.
- [29] S. Brohez, Uncertainty analysis of heat release rate measurement from oxygen consumption calorimetry, *Fire Mater.* 29 (6) (2005) 383–394.
- [30] R.A. Bryant, G.W. Mulholland, A guide to characterizing heat release rate measurement uncertainty for full-scale fire tests, *Fire Mater.* 32 (3) (2008) 121–139.
- [31] S. Brohez, C. Delvosalle, Carbon dioxide generation calorimetry—errors induced by the simplifying assumptions in the standard test methods, *Fire Mater.* 33 (2) (2009) 89–97.
- [32] M. Werrel, J.H. Deubel, S. Krüger, A. Hofmann, U. Krause, The calculation of the heat release rate by oxygen consumption in a controlled-atmosphere cone calorimeter, *Fire Mater.* 38 (2) (2014) 204–226.
- [33] J.P. White, E.D. Link, A.C. Trounev, P.B. Sunderland, A.W. Marshall, J.A. Sheffel, M.L. Corn, M.B. Colket, M. Chaos, H.-Z. Yu, Radiative emissions measurements from a buoyant, turbulent line flame under oxidizer-dilution quenching conditions, *Fire Saf. J.* 76 (2015) 74–84.
- [34] W.M. Thornton, The relation of oxygen to the heat of combustion of organic compounds, *Philos. Mag.* 33 (194) (1917) 196–203.
- [35] C. Huggett, Estimation of rate of heat release by means of oxygen consumption measurements, *Fire Mater.* 4 (2) (1980) 61–65.
- [36] R.N. Walters, S.M. Hackett, R.E. Lyon, Heats of combustion of high temperature polymers, *Fire Mater.* 24 (5) (2000) 245–252.
- [37] A. Tewarson, Generation of heat and gaseous, liquid, and solid products in fires, in: P. DiNenno (Ed.), *SFPE Handbook of Fire Protection Engineering*, fourth ed., National Fire Protection Association, 2008, pp. 109–194.
- [38] M. Elia, T. McDonald, A. Crisp, Errors in measurements of CO₂ with the use of drying agents, *Clin. Chim. Acta* 158 (3) (1986) 237–244.
- [39] C.R. White, S.J. Portugal, G.R. Martin, P.J. Butler, Respirometry: anhydrous Drierite equilibrates with carbon dioxide and increases washout times, *Physiol. Biochem. Zool.* 79 (5) (2006) 977–980.
- [40] W.J. Parker, Calculations of the heat release rate by oxygen consumption for various applications, *J. Fire Sci.* 2 (5) (1984) 380–395.
- [41] M.L. Janssens, Measuring rate of heat release by oxygen consumption, *Fire Technol.* 27 (3) (1991) 234–249.
- [42] A. Tewarson, Heat release rate in diffusion flames, *Thermochim. Acta* 278 (1996) 19–37.
- [43] S. Brohez, C. Delvosalle, G. Marlair, A. Tewarson, Soot generation in fires: an important parameter for accurate calculation of heat release, in: *Fire Safety Science—Proceedings of the Sixth International Symposium, IAFSS, 2000*, pp. 265–276.
- [44] S. Brohez, C. Delvosalle, G. Marlair, A. Tewarson, The measurement of heat release from oxygen consumption in sooty fires, *J. Fire Sci.* 18 (5) (2000) 327–353.
- [45] H. Biteau, T. Steinhaus, C. Schemel, A. Simeoni, G. Marlair, N. Bal, J.L. Torero, Calculation methods for the heat release rate of materials of unknown composition, in: *Fire Safety Science—Proceedings of the Ninth International Symposium, IAFSS, 2008*, pp. 1165–1176.
- [46] W.K. Chow, S.S. Han, Heat release rate calculation in oxygen consumption calorimetry, *Appl. Therm. Eng.* 31 (2) (2011) 304–310.
- [47] F. Takahashi, G.T. Linteris, V.R. Katta, Extinguishment mechanisms of coflow diffusion flames in a cup-burner apparatus, *Proc. Combust. Inst.* 31 (2) (2007) 2721–2729.
- [48] J. Min, F. Baillot, H. Guo, E. Domingues, M. Talbaut, B. Patte-Rouland, Impact of CO₂, N₂ or Ar diluted in air on the length and lifting behavior of a laminar diffusion flame, *Proc. Combust. Inst.* 33 (1) (2011) 1071–1078.
- [49] J. Min, F. Baillot, Experimental investigation of the flame extinction processes of nonpremixed methane flames inside an air coflow diluted with CO₂, N₂, or Ar, *Combust. Flame* 159 (12) (2012) 3502–3517.
- [50] W. Wagner, A. Pruß, The IAPWS formulation 1995 for the thermodynamic properties of ordinary water substance for general and scientific use, *J. Phys. Chem. Ref. Data* 31 (2) (2002) 387–535.
- [51] J.F. Ogilvie, A Monte-Carlo approach to error propagation, *Comput. Chem.* 8 (3) (1984) 205–207.
- [52] J. Galpin, A. Naudin, L. Vervisch, C. Angelberger, O. Colin, P. Domingo, Large-eddy simulation of a fuel-lean premixed turbulent swirl-burner, *Combust. Flame* 155 (1) (2008) 247–266.
- [53] N. Peters, Laminar diffusion flamelet models in non-premixed turbulent combustion, *Prog. Energy Combust. Sci.* 10 (3) (1984) 319–339.
- [54] N. Peters, Laminar flamelet concepts in turbulent combustion, *Proc. Combust. Inst.* 21 (1) (1988) 1231–1250.
- [55] G. Santo, M.A. Delichatsios, Effects of vitiated air on radiation and completeness of combustion in propane pool fires, *Fire Saf. J.* 7 (2) (1984) 159–164.
- [56] J.H. Morehart, E.E. Zukoski, T. Kubota, Characteristics of large diffusion flames burning in a vitiated atmosphere, in: *Fire Safety Science—Proceedings of the Third International Symposium, IAFSS, 1991*, pp. 575–583.
- [57] J.H. Morehart, E.E. Zukoski, T. Kubota, Chemical species produced in fires near the limit of flammability, *Fire Saf. J.* 19 (2) (1992) 177–188.